

Possibilities and Performance of Multi-conjugate Adaptive Optics

THOMAS BERKEFELD¹, ANDREAS GLINDEMANN², STEFAN HIPPLER¹

¹Max-Planck-Institut für Astronomie, ²European Southern Observatory

In order to increase the corrected field of view of an adaptive optics (AO) system, Beckers proposed to place several deformable mirrors (DMs) in the conjugate planes of the dominant turbulent layers (multi-conjugate adaptive optics, MCAO). The wavefront error caused by angular anisoplanatism in an MCAO system depends on the number of corrected modes, the C_n^2 -profile and the geometry of the system. We present a new approach of calculating the anisoplanatism by using spatial correlation functions of (Zernike) modes. We also present a new scheme of measuring the individual wavefront distortion of each of the dominant two layers with one Shack-Hartmann or a Shack-Hartmann-Curvature sensor per guide star using the intensity fluctuations (scintillation) caused by the turbulence. The number and projection geometry of the guide stars are discussed and the corresponding Strehl-numbers are calculated for the measured C_n^2 -profile at the Calar Alto Observatory, Spain, and its 3.5 m telescope. We show that for the Calar Alto 3.5 m telescope, a setup consisting of two deformable mirrors would result in a corrected field of view of three arcminutes.

1 Introduction

While AO systems increase the angular resolution of ground based telescopes by a factor of 5-20, their most severe disadvantage is the very small corrected field of view which is typically of the order of 40 arcseconds in the K-Band ($2.2\mu\text{m}$) and only a few arcseconds in the visible. Placing several DMs in the conjugate planes of the dominant turbulent layers as proposed by Beckers[1] (see fig. 1) has two important advantages over a conventional AO system:

- Correcting the dominant turbulent layers instead of correcting the integrated wavefront aberrations reduces the angular anisoplanatism considerably, even if the turbulence is not located in distinct layers.
- For laser guide star (LGS) systems, focal anisoplanatism can be almost completely eliminated.

Therefore, in order to find the optimal position for the DMs (and for reconstructing the wavefront correctly), the C_n^2 -profile has to be measured simultaneously. The reason for the large isoplanatic patch of an MCAO system compared to that of an AO system can be seen in fig. 2: In an AO system, the DM is placed at the conjugate plane of the entrance pupil, resulting in large light path offsets $d = \theta z$ at high altitudes z . In contrast, MCAO systems minimize the angular anisoplanatism for a given number of DMs by placing them at the conjugate center of height intervalls (weighted by the intervall's turbulence profile), resulting in less overall angular anisoplanatism (compare the size of the shaded areas for both cases). In the case of the Calar Alto C_n^2 -profile, as measured by Klückers et al. (see A.2), the optimal DM conjugate heights are 400 m and 6900 m, which results in a corrected FOV of about 74" radius when five LGSs are used for wavefront sensing, and about 90" for 7 LGSs (see fig. 3).

In section 2, the effects of different geometries of MCAO systems and their laser guide stars on angular anisoplanatism are discussed. The corresponding Strehl-ratios are shown for a 3.5 m telescope and the

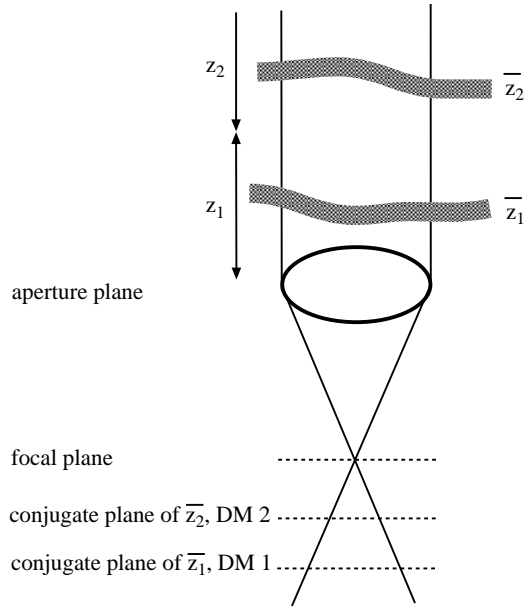


Figure 1: Principle of a 2-DM-MCAO. DM 1 and DM 2 correct the height intervals z_1 and z_2 , respectively.

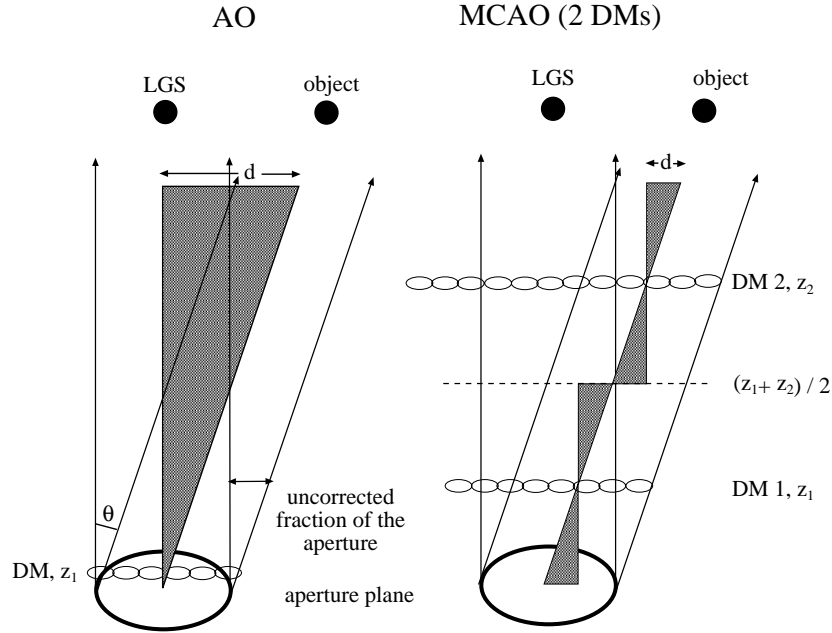


Figure 2: Comparison of an AO and an MCAO system. The shaded areas denote the amount of angular anisoplanatism for a constant (=worst case) C_n^2 -profile. The light path offset $d(z) = \theta|z - z_{DM}|$ causes the angular anisoplanatism and is a function of angle θ between guide star and object and the height difference $|z - z_{DM}|$ to the next DM. The small circles denote the actuators of the DMs placed at the conjugate center of the height intervals.

turbulence profile of the Calar Alto Observatory. Calculating the Strehl-degradation of angular anisoplanatism requires an equation for the wavefront error as a function of the C_n^2 -profile, the number and position of the DMs and the angle between science object and central guide star. This equation, derived in section 3, also allows to optimize the position of each DM (that is to minimize the amount of angular anisoplanatism for a given turbulence profile and number of DMs). The Strehl-ratio as a function of the

angle between object and optical axis for different r_0 and number of corrected modes is shown. The involved (Zernike) correlation functions are listed in A.1. Section 4 gives a short introduction to scintillation and describes the principle of separating the wavefront distortions with a Shack-Hartmann or a Shack-Hartmann-Curvature sensor using intensity fluctuations.

A good introduction of MCAO can be found in [1], more recent estimations of the performance of MCAO systems have been done by Johnston and Welsh [13].

2 Geometrical considerations of MCAO systems

As mentioned before, MCAO systems allow the wavefront correction over a *field* of view instead of only a single direction. For measuring the wavefront distortion, several guide stars are necessary to cover the field. Since it is unlikely to find natural guide stars at the desired positions, laser guide stars (LGS) will be necessary in most cases. For mapping the wavefront distortion over the desired field, the LGSs have to be pointed such that their light cones still overlap at the height of the highest turbulent layer. (see fig. 3 and fig. 4). The field of view of each Shack-Hartmann subaperture must be large enough to cover

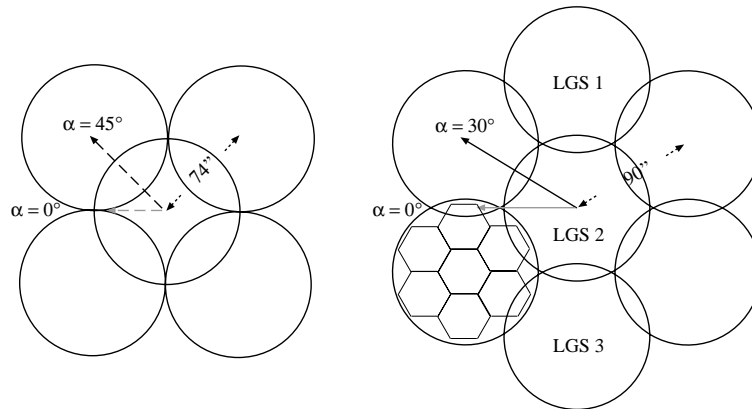


Figure 3: Top view at the highest turbulent layer. Each circle denotes one light cone from an LGS to the telescope. For measuring the wavefront distortion over the desired field of view, the light cones, i.e. the corresponding subapertures of the wavefront sensors have to cover the field of view completely. Five (left) and seven (right) LGSs have been used for the following calculations, respectively. The LGS-numbers are the same as in fig. 4. The viewing angles of fig. 5 and the angular distances between the outer LGSs and the central LGS are also shown.

the images of all LGSs. For NIR observations however the size of the corrected field can reach several arcminutes, requiring a wavefront sensor camera of more than 1k x 1k pixels. In those cases it is more feasible to assign one Shack-Hartmann-array to each LGS.

The amount of overlap (and therefore the corrected field of view) for a given telescope aperture and number of LGSs depends on the C_n^2 -profile and the tolerable remaining anisoplanaticity error. For the Calar Alto C_n^2 -profile, a 3.5 m-class telescope and Near Infrared (NIR) wavelengths lead to a rather small anisoplanatism, so that two DMs would provide good correction over the entire corrected field, whose size should be maximized by a small overlap of neighbouring LGS light cones. For 8 m-class telescopes (seven arcminutes field possible with seven LGSs) or visible wavelengths however, the loss of image quality due to the $(D/r_0)^{5/3}$ -law at the edge of the field becomes severe. Instead of using the full field,

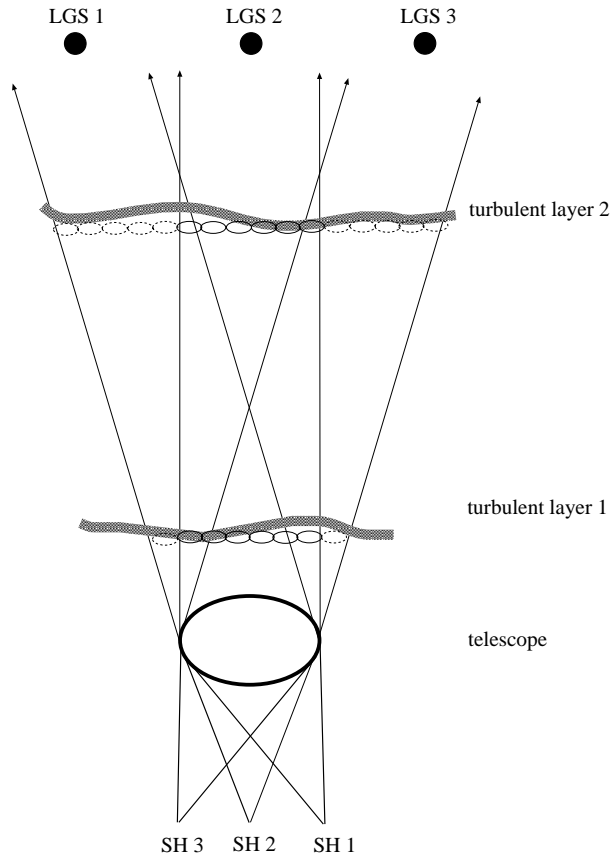


Figure 4: Side view of an MCAO geometry. Each circle in the turbulent layers resembles one Shack-Hartmann-subaperture i.e. one actuator of the DM that is situated in the conjugate plane. Solid and dashed circles denote the correction for the central LGS and the other LGSs, respectively. At low altitudes, off-axis light cones mostly coincide with that of the (optimal corrected) central LGS, whereas at high altitudes, an independent correction of off-axis wavefronts is possible.

the LGSs should be pointed closer together. This results in a higher Strehl number for any direction within the new (smaller) field due to less anisoplanatism of the high altitude correction.

The directions of the LGSs correspond to the highest accuracy for wavefront sensing (as in AO-systems, no angular anisoplanatism). At low altitudes however, the light cones of the LGSs overlap almost completely. Since the corresponding DM can not have more than one shape at the same time, only one direction (usually the central LGS, which signifies the center of the corrected FOV) can be corrected in the optimal way. The angular anisoplanatism of the other LGS directions is mainly due to this low altitude correction, where the light cones mostly overlap with that of the (optimal corrected) central LGS. For high altitudes and little overlap between neighbouring light cones, more degrees of freedom allow a correction close to the optimum, as can be seen in fig. 4. A more evenly correction can be achieved when the low altitude DM corrects the low altitude *average* wavefront error of all LGS directions. This however results in a slight loss of Strehl in the on-axis case. Therefore, in this paper we assume an optimal correction of the field center. Fig. 5 shows the Strehl-ratio as a function of the azimuth angle α and the angular distance between object and central LGS. It is obvious that seven LGSs lead to a larger and more evenly covered field of view than five LGS, although the Strehl dropoff due to residual angular anisoplanatism is slightly higher.

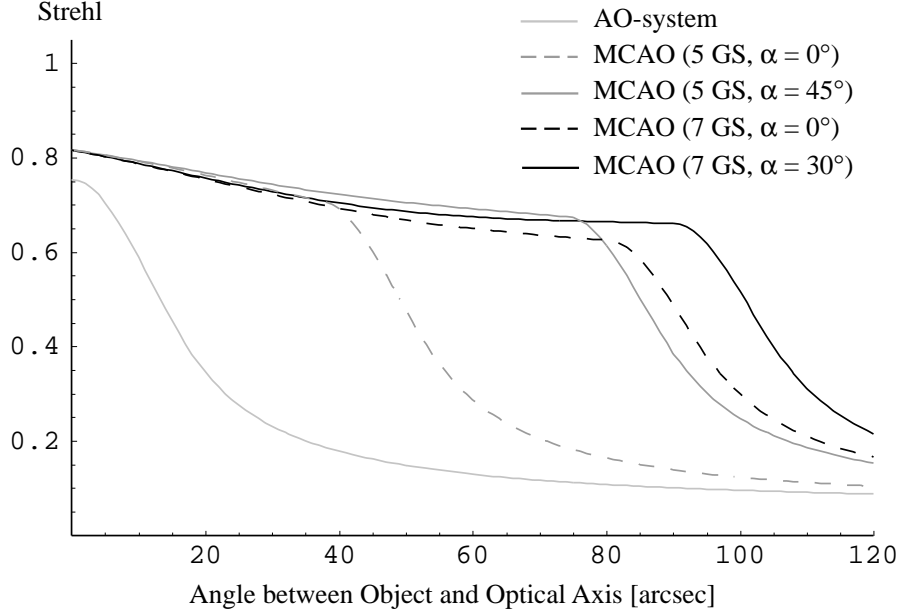


Figure 5: Strehl ($\sigma_{\text{fit}}^2 + \sigma_{\theta}^2 + \sigma_{\text{cone}}^2$, see section 3) as a function of the angle between object and central LGS for the MCAO geometries shown in fig. 3 and a conventional AO system ($D = 3.5$ m, Calar Alto C_n^2 -profile, K-Band, 37 corrected modes). The Strehl-ratio depends both on the azimuth angle α and the distance to the central LGS. The superiority of an MCAO system, especially when seven or more LGSs are used, compared to the conventional AO system is obvious. Due to the cone-effect, the MCAO system gives better performance even at the field center.

Although it is possible to use only one natural guide star (NGS) for absolute tip/tilt determination over the whole field of view, the wavefront reconstruction would not be as accurate as if the absolute tip/tilt was determined for each LGS. Since it is unlikely to find one NGS close to each LGS, the absolute tip/tilt of each LGS should be measured independently. Ragazzoni[20] proposed to position and point auxiliary telescopes in such a way that one LGS and one NGS are in a line with an auxiliary telescope. Then the tip/tilt of each LGS can be determined by subtraction¹. Another possibility is the use of polychromatic LGSs [9], which excite two wavelengths in the sodium layer. The wavelength difference of the two colours leads to a differential tip/tilt caused by atmospheric dispersion, from which the absolute tip/tilt can be calculated. Unfortunately, for a sufficient excitation of the second colour, the output laser power has to be increased by about two orders of magnitude.

3 The error σ_{θ}^2 of angular anisoplanatism

σ_{θ}^2 denotes the wavefront error that is caused by the angle θ between central LGS and science object (angular anisoplanatism). If $\sigma_{\theta}^2 < \sigma_{\theta_0}^2 = 1$, then the object lies inside the *isoplanatic patch* θ_0 and is regarded as corrected [29]. Usually σ_{θ}^2 is expressed as

$$\sigma_{\theta}^2 = \left(\frac{\theta}{\theta_0} \right)^{5/3} \quad (1)$$

¹Since one auxiliary telescope can measure tip *or* tilt, two auxiliary telescopes per LGS are required for absolute tip/tilt-determination.

This equation however does not take the number of corrected modes into account: A simple tip/tilt system has a much larger isoplanatic angle than higher order AO-systems. For the special cases of a tip/tilt system and certain higher order systems Sasiela [26] and Chassat [4] already derived expressions.

The following approach of calculating σ_{θ}^2 is based on the tip/tilt-correlation functions $C_{x,y}$ of two tip/tilt measurements b and b' (see fig. 6) and includes the general dependance of the isoplanatic patch on the degree of correction.

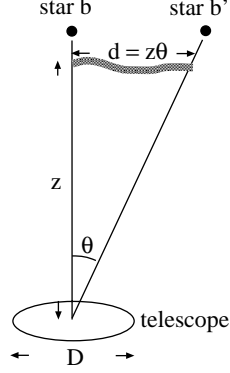


Figure 6: Geometry of the spatial correlation functions ($d =$ light path offset)

Measurements of correlation functions yield important information about the parameters of AO systems: The temporal autocorrelation of tilt measurements determines the necessary bandwidth of the control loop and the correlation of tilt measurements of different stars (spatial correlation) allows the calculation of the isoplanatic angle.

According to Valley [30], the differential jitter of two beams caused by anisoplanatism is

$$\langle (b - b')^2 \rangle_x = 2[1 - C_x] \cdot \langle b^2 \rangle \quad (2)$$

$$\langle (b - b')^2 \rangle_y = 2[1 - C_y] \cdot \langle b^2 \rangle \quad (3)$$

$\langle b^2 \rangle$ represents the one dimensional variance of the tilt[17][14]

$$\langle b^2 \rangle = 0.18 \left(\frac{\lambda}{r_0} \right)^2 \left(\frac{D}{r_0} \right)^{-1/3} \quad [\text{arcsec}^2]. \quad (4)$$

The x- and y- directions correspond to the directions parallel and perpendicular to the line of sight between the two stars. Regarding the two dimensional differential tip/tilt variance as the cause of the wavefront error of the uncorrected wavefront

$$\sigma^2 = 1.03 (D/r_0)^{5/3} = \langle (b - b')^2 \rangle_x + \langle (b - b')^2 \rangle_y \quad (5)$$

leads to an expression for the wavefront difference of the two directions b and b'

$$\sigma_{\theta, \text{uncor}}^2 = 1.03 \left(\frac{D}{r_0} \right)^{5/3} \cdot (2 - C_{x,\theta} - C_{y,\theta}) \quad (6)$$

This equation is valid for uncorrected measurements. If the first N modes are corrected by DMs and/or a tip/tilt-mirror, the different correlation of the individual modes has to be taken into account:

$$\sigma_{\theta}^2 = 2 \left(\frac{D}{r_0} \right)^{5/3} \cdot \sum_{j=1}^N (\sigma_{\text{fit},j-1}^2 - \sigma_{\text{fit},j}^2) (1 - C_j(\theta)) \quad (7)$$

The factor of two resembles the two statistical variables (object and guide star). The sum considers the different correlation C_j of each mode j and its contribution $\sigma_{\text{fit},j-1}^2 - \sigma_{\text{fit},j}^2$ (see A.3) to the total wavefront error σ_{θ}^2 . This equation is in good agreement with Chassat[4] for Zernike-polynomials, but can be used with other sets of polynomials and any number of corrected modes as well.

For a simple tip/tilt-system one obtains

$$\sigma_{\theta,\text{tilt}}^2 = 0.896 \left(\frac{D}{r_0} \right)^{5/3} (2 - C_x(\theta) - C_y(\theta)). \quad (8)$$

As a consequence of the approximation of a simple control loop, an improvement of the image quality can only be expected for correlations better than 0.5 (a bad correction is worse than no correction.).

For a system with laser guide stars the wavefront error σ_{θ}^2 becomes

$$\sigma_{\theta,\text{LGS}}^2 = \left(\frac{D}{r_0} \right)^{5/3} [0.896 \cdot (2 - C_x(\theta_{\text{NGS}}) - C_y(\theta_{\text{NGS}})) + \quad (9)$$

$$2 \sum_{j=3}^N (\sigma_{\text{fit},j-1}^2 - \sigma_{\text{fit},j}^2) (1 - C_j(\theta_{\text{LGS}}))]. \quad (10)$$

3.1 Angular Anisoplanatism of a conventional AO-system

Since the turbulence profile dependence of the above equations is hidden in the correlation functions C_j , it is sufficient to measure the tip/tilt correlation functions for calculating \mathfrak{C}_{θ}^2 . Higher order correlations can be roughly derived from the tip/tilt correlations, as described in A.1. If the C_n^2 -profile is known, the isoplanatic angle can be calculated using

$$C_j(\theta) = \frac{\int c_j(z\theta) C_n^2(z) dz}{\int C_n^2 dz}, \quad (11)$$

where $c_j(z\theta) = c_j(d)$ denotes the correlation caused by a single layer at height z . This equation is valid for uncorrected imaging or an AO system with the DM situated in the conjugate plane of the aperture. Fig. 7 shows the Strehl-number of $\sigma_{\text{fit}}^2 + \sigma_{\theta}^2$ as a function of the number of corrected modes and the angle between science object and guide star. Because of the fast decorrelation of the higher modes, a low order correction can yield a higher Strehl at large distances between object and guide star. The isoplanatic angle of typically about 20 arcseconds is in good agreement with measurements done at the Calar Alto 3.5 m-telescope using the AO-system ALFA [15].

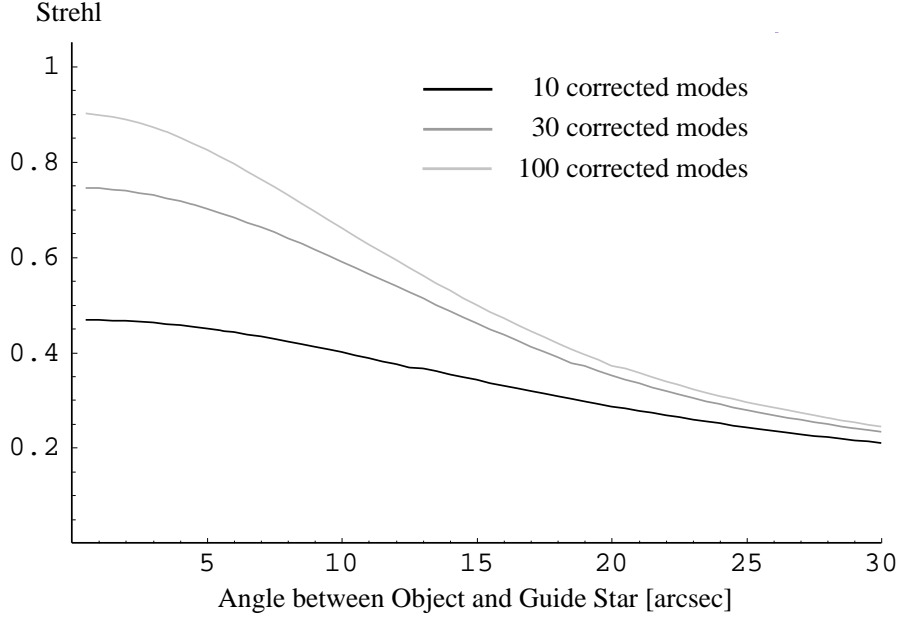


Figure 7: Strehl ($\sigma_{\text{fit}}^2 + \sigma_{\theta}^2$) of an AO system as a function of the number of corrected modes and the angle between science object and guide star ($D = 3.5$ m, Calar Alto C_n^2 -profile)

3.2 Angular Anisoplanatism of a 2-DM-MCAO-system

In the case of an AO or MCAO system with M DMs at conjugated heights z_i , the correlation C_j becomes

$$C_j(\theta) = \left(\sum_{i=1}^M \int_{(z_{i-1}+z_i)/2}^{(z_i+z_{i+1})/2} c_j(|z_i - z|\theta) C_n^2(z) dz \right) / \int_0^{\infty} C_n^2(z) dz, \quad (12)$$

where $(z_0 + z_1)/2 = 0$ (the integration ranges from the ground to the first mirror) and $(z_M + z_{M+1})/2 =$ height of the highest turbulent layer. For simplification it has been assumed that the number of corrected modes per aperture size is the same in all layers, i.e. DMs correcting the high altitude turbulence have to correct more modes (because of the larger covered area) than the low altitude DMs. Due to the smaller light path offset between object and guide star in an MCAO system, the correlation functions have higher values than those of AO systems (see fig. 2). Inserting C_j in eq. 7 delivers the angular anisoplanatism σ_{θ}^2 of an MCAO system². Usually the science object does not coincide with an LGS, so different parts of the wavefront intersect different LGS light cones and are corrected accordingly. In this paper, the contribution of each intersection to angular anisoplanatism is weighted linearly by the intersection fraction (normalized to the aperture). This approximation leads to a linear Strehl decrease close to the field center (instead of the almost gaussian decrease for AO systems), see fig. 8 and fig. 9.

Because already a 2-DM-MCAO system provides a very wide and well corrected field of view in K-band (see fig. 5) and it is the simplest and cheapest MCAO possible, the following calculations have been performed for a 2-DM-MCAO system. Fig. 8 and 9 show the Strehl-ratio ($\sigma_{\text{fit}}^2 + \sigma_{\theta}^2$) of an MCAO (2 DMs) as a function of the number of corrected modes and r_0 and the angle between science object and guide star. It is obvious that a high order correction at large angles θ results in more Strehl-gain in MCAO than in AO systems. It has been assumed, that the absolute tip/tilt of the LGSs is known (see end

²If the tip/tilt is measured by an NGS, j runs from 3 to N . In this case, σ_{θ}^2 is determined by eq. 8.

of section 2). Due to the $(D/r_0)^{(5/3)}$ -law (see eq. 7), both AO and MCAO systems heavily depend on good seeing to reach a high image quality.

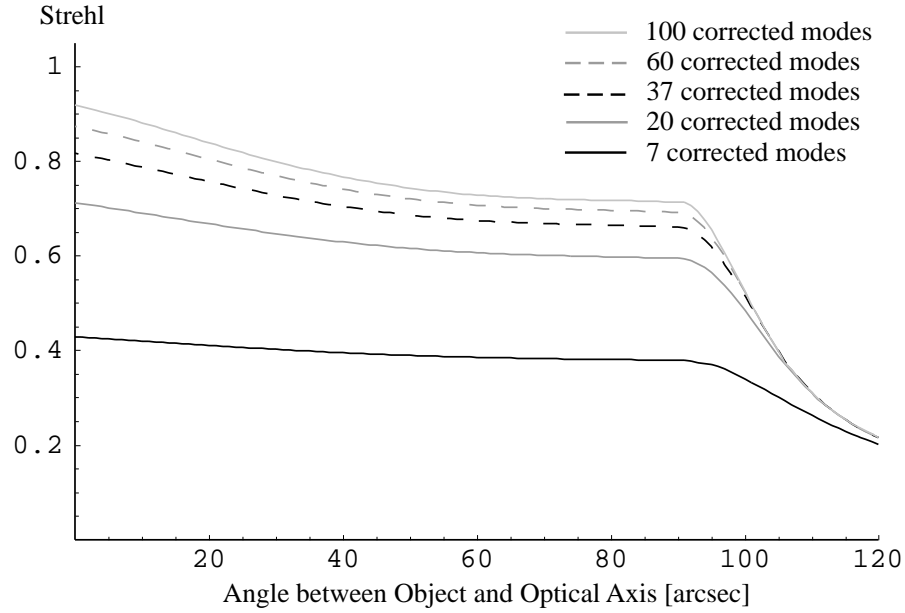


Figure 8: Strehl ($\sigma_{\text{fit}}^2 + \sigma_{\theta}^2$) of an MCAO (2 DMs) as a function of the number of corrected modes and the angle between science object and optical axis ($D = 3.5$ m, 37 corrected modes, Calar Alto C_n^2 -profile, K-Band, $\alpha = 30^\circ$ (see fig. 3)).

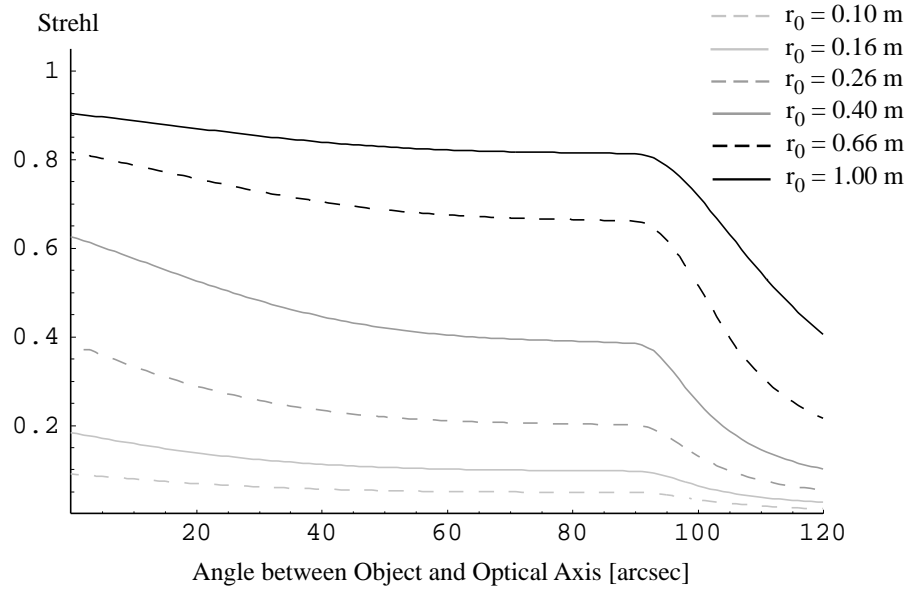


Figure 9: Strehl ($\sigma_{\text{fit}}^2 + \sigma_{\theta}^2$) of an MCAO (2 DMs) as a function of r_0 (scaled Calar Alto C_n^2 -profile) and the angle between science object and optical axis ($D = 3.5$ m, 37 corrected modes, $\alpha = 30^\circ$ (see fig. 3)).

Another possibility of calculating the isoplanatic angle of MCAO systems can be found in [28] and [31]. Their solution however is independent of the aperture size and the number of corrected modes.

4 Separating the wavefront distortion of high and low altitude turbulent layers

As it has been shown in the previous section, a 2-DM-MCAO already produces a wide and relatively even corrected field of view. It is therefore sufficient to distinguish the wavefront aberrations of the corresponding two layers (usually a high and a low altitude layer) or height intervals.

One possibility is the use of tomographic methods, as proposed by Beckers [1]. Since a large number of LGSs is required, this method will be quite demanding at night telescopes, but can be very useful at solar telescopes where no LGSs are needed. New aspects of zonal tomography can be found in a paper by Tallon and Foy [27], the possibility of modal tomography has recently been shown by Ragazzoni [21].

In order to avoid additional LGSs for measuring the individual wavefront distortion of two turbulent layers, the intensity information provided in each lenslet of a Shack-Hartmann sensor can be used.

Other aspects of wavefront separation and reconstruction can be found in [25, 12, 23, 11].

4.1 Introduction to scintillation

Intensity fluctuations of star images (scintillation) are caused by the curvature of turbulent layers (second deviation of the phase, lensing effect, as shown in fig. 10). Usually astronomical observations are

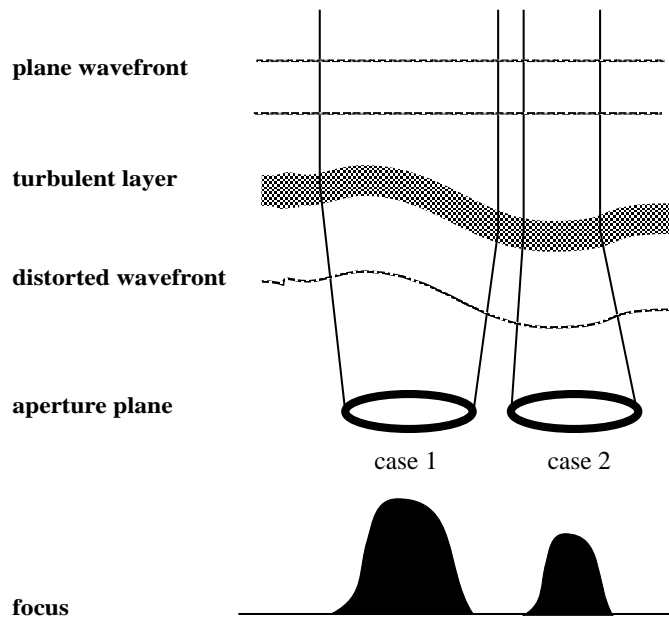


Figure 10: A turbulent layer focuses (case 1) or defocuses (case 2) the incoming light, resulting in a larger or smaller effective aperture in the focal plane.

not affected by scintillation because of the long integration times. However, if intensity fluctuations of highly time-resolved measurements are not treated as noise, their height dependance can be used to provide information about the height distribution of turbulent layers. Good Introductions to the theory of scintillation can be found in[5][6][7][8][22].

The variance of the measured intensity σ_I^2 consists of the variance of the scintillation σ_S^2 and the other noise sources (detector noise σ_D^2 and photon noise σ_P^2):

$$\sigma_I^2 = \sigma_S^2 + \sigma_D^2 + \sigma_P^2 \quad (13)$$

For known detector noise and photon noise, the measurement determines the amount of scintillation. According to Reiger [22], the theoretical value of σ_S^2 is given by

$$\sigma_S^2 \propto D^{-7/3} (\cos \gamma)^{-3} \int z^2 C_n^2(z) dz, \quad (14)$$

D and γ denoting the telescope aperture and the zenith angle, respectively. Simulations with the program *Turbulence* [2] have lead to the normalized variance of the intensity

$$\sigma_S^2 = D^{-7/3} \lambda^2 z^2 r_0^{-5/3} (\cos \gamma)^{-3} \quad (15)$$

for a single layer at height z and Fried parameter r_0 . Because of $r_0 \propto \lambda^{6/5}$, the scintillation does not depend on the wavelength. For a C_n^2 -profile one obtains

$$\sigma_S^2 = 16.7 \cdot D^{-7/3} (\cos \gamma)^{-3} \int z^2 C_n^2(z) dz. \quad (16)$$

Due to the factor z^2 the scintillation is mostly caused by high altitude turbulent layers. For $\sigma_S > 10\%$, i.e. high zenith angles or small telescope apertures, the scintillation begins to become nonlinear, approaching a maximum value, and eq. 16 is no longer valid [5][19].

4.2 Optical setup for separating the contributions of high and low altitude turbulent layers

Since the wavefront gradient in each Shack-Hartmann (SH) subaperture is the *sum* of the wavefront distortions of turbulent layers, additional information is needed for distinguishing the influence of individual layers. By using the intensity information provided by the SH sensor, the distortion of one of the layers can be reconstructed. Together with the known sum of the aberrations, this defines the wavefront distortion of the other layer (fig. 11):

As in a conventional AO-setup, the SH sensor measures the tip/tilt in each subaperture, thus delivering the integrated wavefront error. Because the SH sensor is situated in the conjugate plane of one of the turbulent layers (subsequently named first layer), this layer has no effect on the intensity of the SH pattern. The - according to the SH sensor - defocused other (subsequently named second) layer leads to intensity fluctuations $I_2'(x_2')$ in the subapertures from which the wavefront distortion ϕ of the second layer can be reconstructed [24] [11]:

$$I_2'(x_2') = 1 - \frac{z_2' - z_1'}{2k} \frac{\partial^2 \phi_1(x_2')}{\partial x_2'^2} \quad (17)$$

Again, numbers denote the layers. z resembles the height, $k = 2\pi/\lambda$, and dashed variables signify the conjugate planes. The radial wavefront tilt affects the intensity measurement at the edge of the aperture[25].

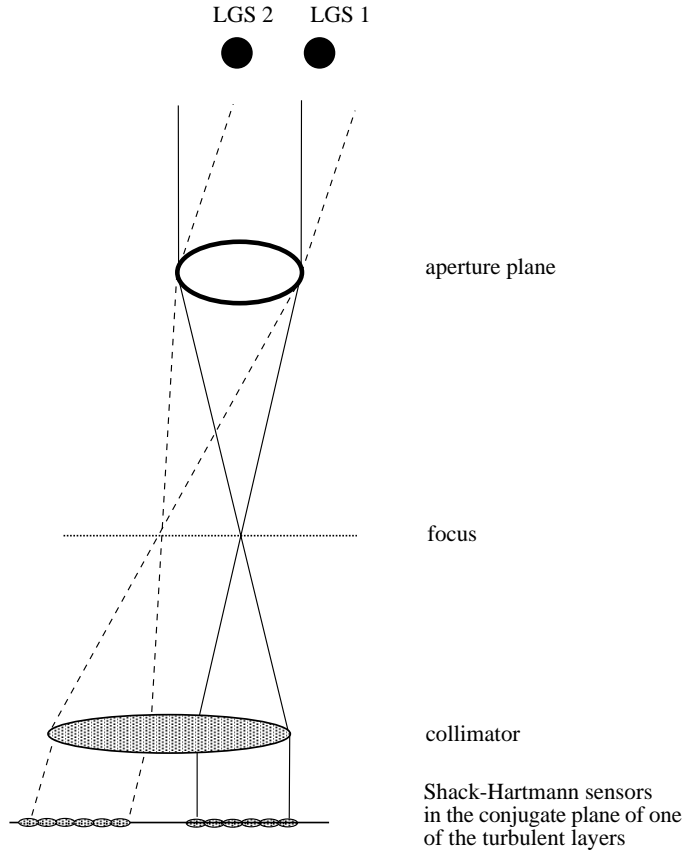


Figure 11: Setup of a wavefront sensor separating the wavefront distortions of two turbulent layers. For clarity, the light paths of only two guide stars have been plotted. One SH sensor per LGS is required.

Although it can be extracted directly from the SH tilt measurement and thus its contribution can easily be corrected, the edge radial tilts must be known for each layer. They can be estimated by first determining the mean gradient m_i (averaged over all LGSs j) of each edge subaperture i . The m_i can be regarded as the edge gradients of the low altitude turbulence (which are the same for all LGSs), whereas the deviation r_{ij} can be seen as the high altitude gradients

$$r_{ij} = t_{ij} - m_i \quad \text{with} \quad m_i = \frac{\sum_{j=1}^n t_{ij}}{n}, \quad (18)$$

with t_{ij} being the measured gradients. It is obvious that this is only an approximation which will be the more accurate the higher the number of LGS (and thus the corrected field of view) is. Once the wavefront distortion of one of the layers has been reconstructed, subtraction from the measured sum of the wavefront errors delivers the wavefront distortion of the other layer. The error made by the estimation of the radial gradients, as described above, is still unknown. This problem should therefore be addressed more closely.

The normalized mean square error (MSE) of the intensity measurement is proportional to the wavefront error induced by the inaccurate intensity measurement and can be written as

$$\text{MSE} = \frac{\frac{1}{N_y} + \frac{n \cdot R^2}{N_y^2} + 16.7 \cdot D_{\text{sub}}^{-7/3} (\cos \gamma)^{-3} \int_{l_1} (z-h)^2 C_n^2(z) dz}{16.7 \cdot D_{\text{sub}}^{-7/3} (\cos \gamma)^{-3} \int_{l_2} (z-h)^2 C_n^2(z) dz} \quad (19)$$

The numerator and the denominator resemble the noise and the signal, respectively. The noise consists of the photon noise $N^{1/2}$ and the read noise $R \cdot n^{1/2}$ (n being the number of pixels used for the intensity measurements, R denotes the readout noise per pixel). For the scintillation signal, h is the conjugate height of the SH sensor and D_{sub} the subaperture size of the SH sensor. The scintillation error due to the non discrete layering of the C_n^2 -profile is very small and need not be taken into account.

Typically the measured scintillation is of the order of a few percent. This poses problems at low light levels where the scintillation competes with the shot noise. Although it is possible to measure the scintillation of the more turbulent layer (usually the ground layer) and thus get a smaller relative error, this does not lead to a better separation of the layers because the *absolute* error of the wavefront reconstruction is also proportional to the turbulence strength. Therefore it does not matter whether the scintillation of the strong or the weak turbulence is measured. Instead, the MSE can be reduced by moving the SH sensor further away from the conjugate plane of the first turbulent layer, as shown in Fig. 12: Although this

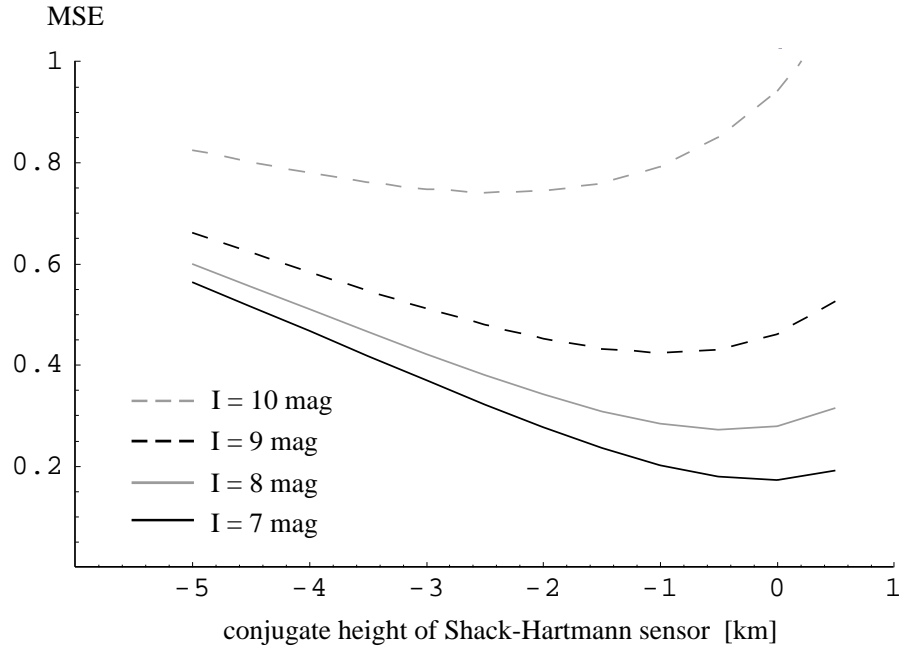


Figure 12: Normalized mean square error (MSE) of the intensity measurements as a function of the conjugate height of the SH sensor for different LGS intensities. The subaperture size and the read noise have been assumed as $D_{\text{sub}} = 0.5$ m (35-40 corrected modes) and $R = 3e^-$, which are typical values for ALFA. The integration time of the wavefront sensor was chosen to be optimal for each LGS brightness. In this figure, the scintillation caused by the high altitude turbulence is measured. Increasing LGS brightness leads to increasing optimal height of the SH sensor.

leads to an unwanted contribution to scintillation from the now defocused first layer, the MSE decreases within certain limits due to the much higher scintillation signal from the second layer. However, in the

case of a 589 nm LGS with a 10 mag G-star brightness equivalent, the maximum accuracy is 0.75, which is not sufficient for wavefront separation with one SH sensor.

For low light levels the amount of scintillation has to be increased by moving the SH sensor further away from the conjugate planes of the turbulent layers. Since the scintillation effects of two layers cannot be distinguished with one SH sensor, an additional SH sensor is necessary, leading to the *Shack-Hartmann-Curvature (SHC) sensor*. In contrast to the SHC setup with two SH sensors placed in the conjugate planes of the two turbulent layers (Glindemann and Berkefeld [10]), we propose to position the SH sensors to deliver mean intensity fluctuations of 10% each (non-linearity limit of scintillation). This is the case at the conjugate planes of a very large positive height and a large negative height, leading to an excess of illumination in one plane and to a lack of illumination in the other, similar to the Curvature Sensor [25]. For the Calar Alto C_n^2 -profile this results in heights of approx. 16 km and -12 km. The mean square error becomes

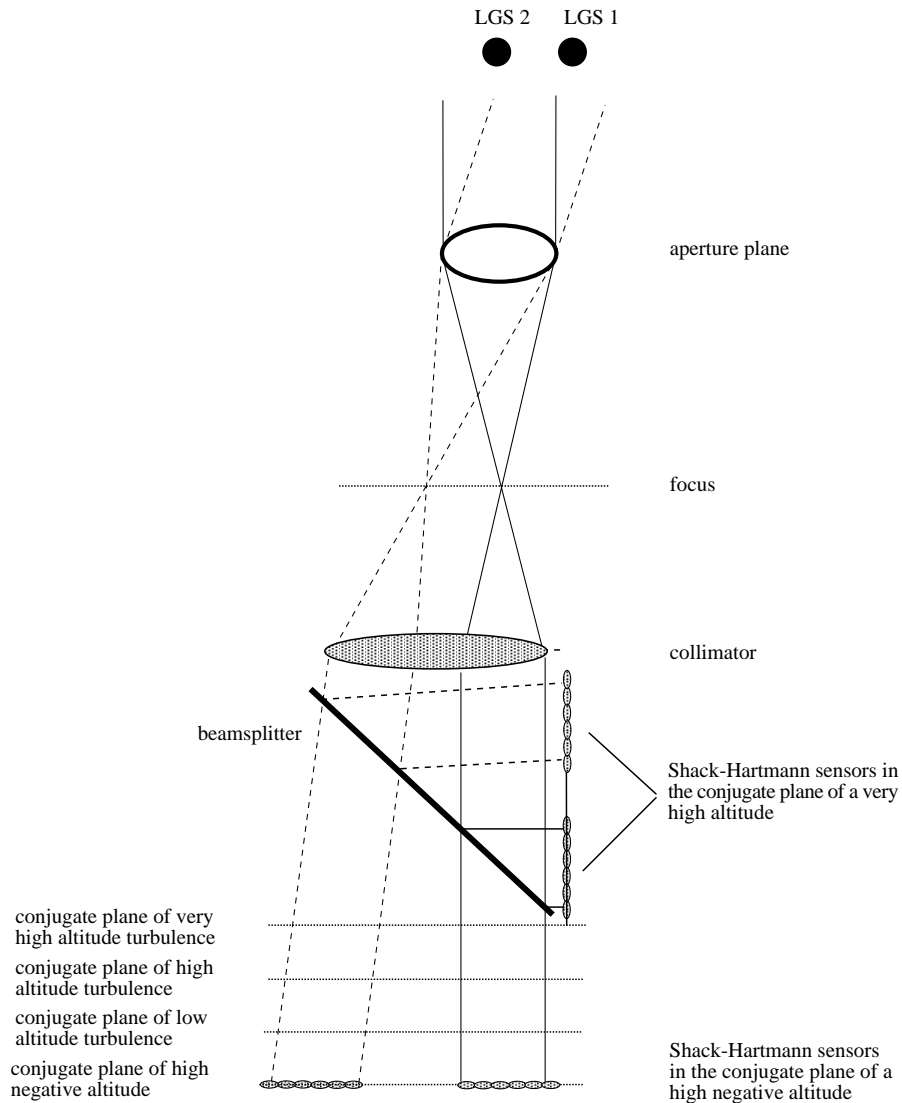


Figure 13: Setup of a Shack-Hartmann-Curvature sensor separating the wavefront distortions of two turbulent layers (low light level). For clarity, the light paths of only two guide stars have been plotted. One SHC sensor per LGS is required.

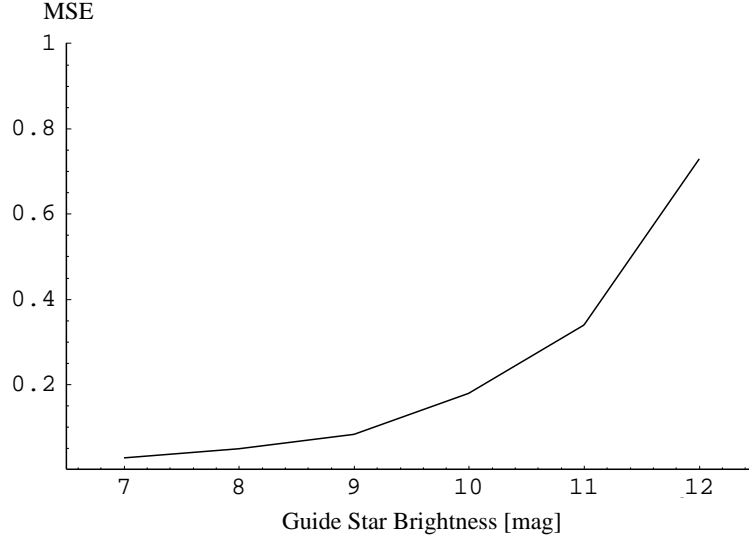


Figure 14: Normalized mean square error (MSE) of the intensity measurements performed by a SHC-sensor as a function of the guide star brightness. The conjugate heights of the SH sensors have been assumed as 16 km and -12 km, the other parameters are the same as in fig 12.

$$\text{MSE} = \frac{\frac{1}{16.7 \cdot D_{\text{sub}}^{-7/3} (\cos \gamma)^{-3}} \cdot \left(\frac{1}{N_{\gamma}} + \frac{n \cdot R^2}{N_{\gamma}^2} \right)}{\left| \int_{l_1} ((z - \text{SH}_1)^2 + (z - \text{SH}_2)^2) C_n^2(z) dz - \int_{l_2} ((z - \text{SH}_1)^2 + (z - \text{SH}_2)^2) C_n^2(z) dz \right|}. \quad (20)$$

An LGS brightness of 10mag leads to an accuracy of 0.2 which should be sufficient for most applications. Therefore observations in the NIR and a typical LGS brightness of 10 mag require one Shack-Hartmann-Curvature sensor (consisting of two SH sensors) per LGS. Observations in the visible require much more powerful LGSs in order to sense and correct a higher number of modes. Then a single SH per LGS can be used. In any case, the C_n^2 -profile and the zenith angle should be monitored continuously in order to adjust the SH sensors and the DMs accordingly.

5 Conclusion

By using MCAO, it is possible to overcome the most severe disadvantage of AO, the very small corrected FOV. We have shown how the geometry of MCAO systems affects the angular anisoplanatism and thus the size of the corrected FOV. A setup with seven LGSs for wavefront sensing leads to a wide and relatively evenly corrected field. In the case of the Calar Alto 3.5 m telescope, this setup would lead to a FOV of three arcminutes. Eq. 7 plays an important role in calculating the wavefront error caused by angular anisoplanatism. By its minimization one obtains the optimal position of the DMs (according to the C_n^2 -profile). Since the remaining anisoplanatism inside the field is rather small, a wavefront correction with two DMs seems to be a good compromise between the anisoplanatism and the costs and the complexity of the system. The separation of the wavefront errors of the two layers can be accomplished in various ways: For solar telescopes, tomographic methods, as proposed by Beckers, seem to be the most accurate and easy to implement way. At night telescopes, the separation can be done by using the intensity information provided by each lenslet of the SH sensor. In the case of low light levels (10 mag LGS, typical for

NIR observations) one Shack-Hartmann-Curvature sensor per LGS must be used, whereas one SH sensor per LGS is sufficient for the bright LGSs required by high order AO systems working in the visible.

The high costs for the LGS setup and the absolute tip/tilt determination will prevent MCAO systems being used at existing 3.5 m-class-telescopes, at least as long as other further improvements of conventional AO systems are possible. At 8+ m-class-telescopes however, focal anisoplanatism will require the use of multiple laser guide stars. Furthermore, the costs of MCAO systems compared to those of the telescope will decrease, so that MCAO will become a common feature at large telescopes.

A Appendix

A.1 Spatial correlation of Zernike-modes

The definition of the normalized correlation c of two measurements b and b' is [3], see fig. 6:

$$c = \frac{\langle bb' \rangle - \langle b \rangle \langle b' \rangle}{\sqrt{(\langle b \rangle^2 - \langle b^2 \rangle)(\langle b' \rangle^2 - \langle b'^2 \rangle)}} \quad (21)$$

In the case of tilt measurements, eq. 21 can be simplified: Since $\langle b \rangle = \langle b' \rangle = 0$ (the mean tilt is zero) and $\langle b^2 \rangle = \langle b'^2 \rangle$, c can be written as

$$c = \frac{\langle bb' \rangle}{\langle b^2 \rangle}. \quad (22)$$

For a single turbulent layer (fig. 6), Valley [30] derived an expression for the correlation of Zernike-modes:

$$\begin{aligned} c_{nm}^{nm} &\propto \int dz z^{-14/3} \cdot J_0(2zd/D) \cdot J_{2n+|m|+1}^2(z) \\ c_{n-m}^{nm} &\propto (-1)^m \int dz z^{-14/3} \cdot J_{|2m|}(2zd/D) \cdot J_{2n+|m|+1}^2(z), \end{aligned} \quad (23)$$

m and $2n + |m|$ denote the azimuthal and radial order of the Zernike modes. The correlation depends on the telescope aperture D and the light path offset d , but because of the normalization, it is independent of the turbulence strength of the layer. With the mode ordering function j

$$\begin{aligned} j &= (2n+1)n && \text{for } m = 0 \\ j &= (2n+|m|+1)(2n+|m|)/2+m-1 && \text{for } m > 0 \\ j+1 &= (2n+|m|+1)(2n+|m|)/2+m && \text{for } m > 0 \end{aligned} \quad (24)$$

one obtains the correlation of the Zernike mode j

$$\begin{aligned} c_j(d) &= c_{(2n+1)(2n)/2}(d) &= \frac{c_{nm}^{nm}(d/D)}{c_{nm}^{nm}(0)} && \text{for } m = 0 \\ c_j(d) &= c_{(2n+|m|+1)(2n+|m|)/2+m-1}(d) &= \frac{c_{nm}^{nm}(d/D) + c_{n-m}^{nm}(d/D)}{c_{nm}^{nm}(0) + c_{n-m}^{nm}(0)} && \text{for } m \neq 0 \\ c_{j+1}(d) &= c_{(2n+|m|+1)(2n+|m|)/2+m}(d) &= \frac{c_{nm}^{nm}(d/D) - c_{n-m}^{nm}(d/D)}{c_{nm}^{nm}(0) - c_{n-m}^{nm}(0)} && \text{for } m \neq 0 \end{aligned} \quad (25)$$

Figure 15 shows the correlation for different aberrations as a function of the parameter d/D . Higher order aberrations generally decorrelate faster because they resemble smaller structures (and thus smaller correlation lengths).

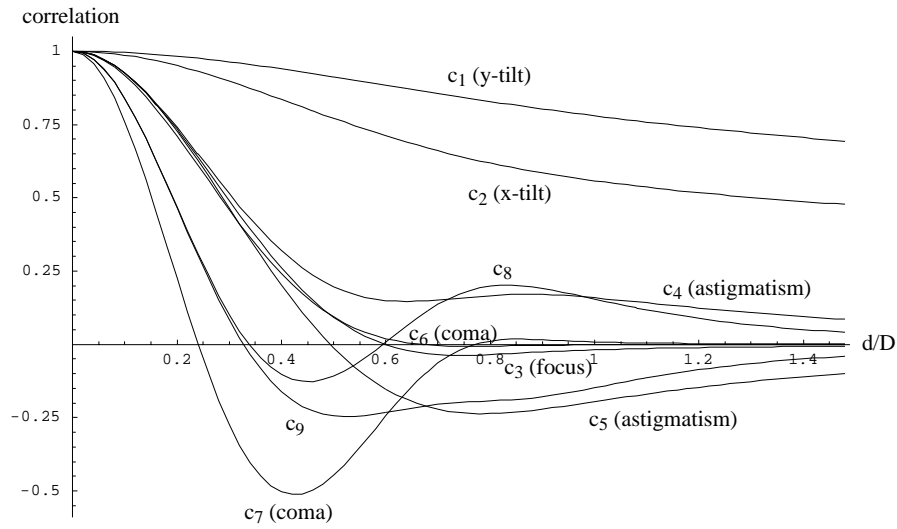


Figure 15: Correlation for the first Zernike-modes as a function of the light path offset d and the aperture D

A.2 Calar Alto C_n^2 -profile

Fig. 16 shows a slightly simplified C_n^2 -profile measured by Klückers et al. [16] at the Calar Alto Observatory, Spain. The upper turbulent layer at 7 km height delivers the main contribution to the angular anisoplanatism, the lower turbulent layer determines most of η_0 . For a 2-DM-MCAO, the optimal DM-heights are 400 m and 6900 m. It should be noted, that the turbulence profile can change rather quickly. Klückers reported a change of the upper turbulent layer strength by a factor of two in only a few minutes. Therefore, frequent C_n^2 -measurements should be made to adjust the optimum height of the DMs.

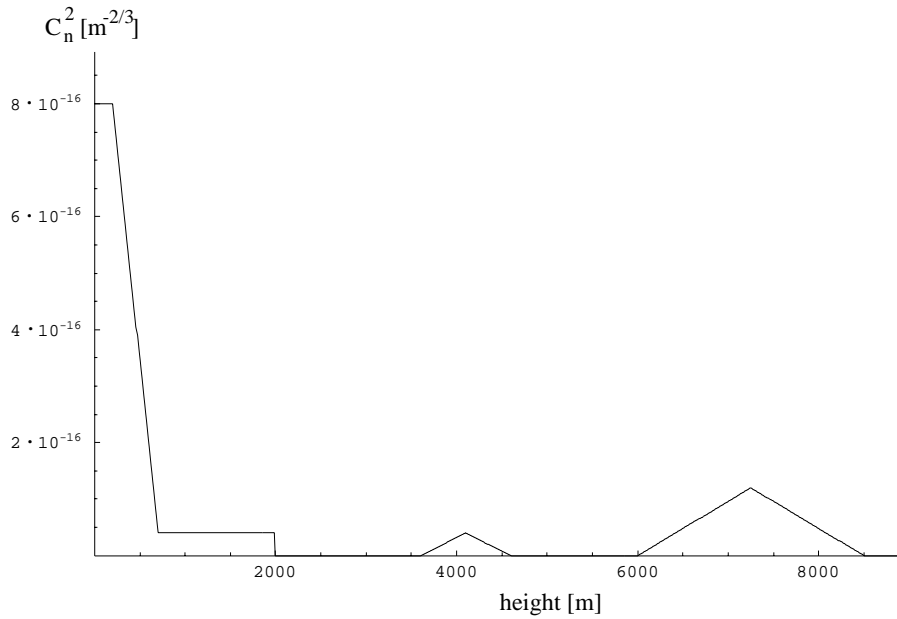


Figure 16: C_n^2 -profile at the Calar Alto Observatory (Klückers et al., $r_0 = 66$ cm at K-Band)

A.3 The fitting error σ_{fit}^2

σ_{fit}^2 denotes the wavefront error made by using a finite number of polynomial modes for describing the wavefront. Table 1 shows σ_{fit}^2 for Kolmogorov-turbulence described by Zernike-polynomials as a function of the number j of corrected modes[18].

$\sigma_{\text{fit},0}^2 = 1.0299(D/r_0)^{5/3}$	$\sigma_{\text{fit},7}^2 = 0.0525(D/r_0)^{5/3}$	$\sigma_{\text{fit},14}^2 = 0.0279(D/r_0)^{5/3}$
$\sigma_{\text{fit},1}^2 = 0.5820(D/r_0)^{5/3}$	$\sigma_{\text{fit},8}^2 = 0.0463(D/r_0)^{5/3}$	$\sigma_{\text{fit},15}^2 = 0.0267(D/r_0)^{5/3}$
$\sigma_{\text{fit},2}^2 = 0.1340(D/r_0)^{5/3}$	$\sigma_{\text{fit},9}^2 = 0.0401(D/r_0)^{5/3}$	$\sigma_{\text{fit},16}^2 = 0.0255(D/r_0)^{5/3}$
$\sigma_{\text{fit},3}^2 = 0.1110(D/r_0)^{5/3}$	$\sigma_{\text{fit},10}^2 = 0.0377(D/r_0)^{5/3}$	$\sigma_{\text{fit},17}^2 = 0.0243(D/r_0)^{5/3}$
$\sigma_{\text{fit},4}^2 = 0.0880(D/r_0)^{5/3}$	$\sigma_{\text{fit},11}^2 = 0.0352(D/r_0)^{5/3}$	$\sigma_{\text{fit},18}^2 = 0.0232(D/r_0)^{5/3}$
$\sigma_{\text{fit},5}^2 = 0.0648(D/r_0)^{5/3}$	$\sigma_{\text{fit},12}^2 = 0.0328(D/r_0)^{5/3}$	$\sigma_{\text{fit},19}^2 = 0.0220(D/r_0)^{5/3}$
$\sigma_{\text{fit},6}^2 = 0.0587(D/r_0)^{5/3}$	$\sigma_{\text{fit},13}^2 = 0.0304(D/r_0)^{5/3}$	

Table 1: Wavefront error for Kolmogorov-turbulence described by Zernike-polynomials as a function of the number j of corrected modes

For $j > 20$, σ_{fit}^2 can be approximated by

$$\sigma_{\text{fit},j}^2 \approx 0,2944(j+1)^{-\sqrt{3}/2}(D/r_0)^{5/3}. \quad (26)$$

References

- [1] J.M. Beckers. ESO-symposium on large telescopes and their instrumentation. *ESO-Proceedings*, page 693, 1988.
- [2] T. Berkefeld, A. Glindemann, and R. Weis. in preparation.
- [3] I.N. Bronstein and K.A. Semendjajew. *Taschenbuch der Mathematik*. Verlag Harri Deutsch, 1987.
- [4] F. Chassat. Calcul du domaine d’isoplanétisme d’un système d’optique adaptative fonctionnant à travers la turbulence atmosphérique. *J. Optics, Paris*, 20:13, 1989.
- [5] D. Dravins, L. Lindegren, E. Mezey, and A.T. Young. Atmospheric intensity scintillation of stars i. statistical distributions and temporal properties. *Publ. Astron. Soc. Pac.*, 109:173, 1997.
- [6] D. Dravins, L. Lindegren, E. Mezey, and A.T. Young. Atmospheric intensity scintillation of stars ii. dependence on optical wavelengths. *Publ. Astron. Soc. Pac.*, 109:725, 1997.
- [7] D. Dravins, L. Lindegren, E. Mezey, and A.T. Young. Atmospheric intensity scintillation of stars iii. effects for different telescope apertures. *Publ. Astron. Soc. Pac.*, 110:610, 1998.
- [8] H. Elsässer and H. Siedentopf. Zur Theorie der astronomischen Szintillation. i. *Zeitschrift für Astrophysik*, 48:213, 1959.
- [9] R. Foy, A. Migus, F. Biraben, G. Grynberg, P.R. McCullough, and M. Tallon. The polychromatic artificial sodium star: A new concept for correcting the atmospheric tilt. *Astronomy & Astrophysics supplement series*, 111:569, 1995.

- [10] A. Glindemann and T. Berkefeld. A new method for separating atmospheric layers using a shack-hartmann curvature sensor. In *Adaptive Optics*, volume 13, page 153. OSA Technical Digest Series, 1996.
- [11] A. Glindemann, S. Hippler, T. Berkefeld, and W. Hackenberg. Adaptive optics on large telescopes. *Experimental Astronomy*, 2000.
- [12] P. Hickson and G. Burley. Single-image wavefront curvature sensing. *SPIE*, 2201:549, 1994.
- [13] D.C. Johnston and B.M. Welsh. Analysis of multiconjugate adaptive optics. *J. Opt. Soc. Am.*, 11:394, 1994.
- [14] M. Kasper. Dissertation Universität Heidelberg, 2000.
- [15] Markus Kasper. private communications.
- [16] V.A. Klückers, N.J. Wooder, T.W. Nichols, M.J. Adcock, I. Munro, and J.C. Dainty. Profiling of atmospheric turbulence strength and velocity using a generalised SCIDAR technique. *A & A Supplement Series*, 130:141, 1998.
- [17] H.M. Martin. Image motion as a measure of seeing quality. *Publ. Astron. Soc. Pac.*, 99:1360, 1987.
- [18] R.J. Noll. Zernike polynomials and atmospheric turbulence. *J. Opt. Soc. Am.*, 66:211, 1976.
- [19] W.M. Protheroe. Preliminary Report on Stellar Scintillation. *Ohio State University*, 4, 1954.
- [20] R. Ragazzoni. Absolute tip-tilt determination with laser beacons. *Astronomy & Astrophysics*, 305:L13, 1996.
- [21] Roberto Ragazzoni, Enrico Marchetti, and Francois Rigaut. Modal tomography for adaptive optics. *Astronomy and Astrophysics*, 342:L53, 1999.
- [22] S.H. Reiger. Starlight Scintillation and Atmospheric Turbulence. *AJ*, 68:395, 1963.
- [23] E.N. Ribak. Stellar scintillations as a remote atmospheric wave-front sensor. *Opt. Letters*, 21:435, 1996.
- [24] E.N. Ribak and E. Gershnik. Stellar scintillation as a remote atmospheric wave-front sensor. *Optics Letters*, 21,6:435, 1996.
- [25] F. Roddier. Curvature sensing and compensation: a new concept in adaptive optics. *Applied Optics*, 27,7:1223, 1988.
- [26] R.J. Sasiela and J.D. Shelton. Transverse spectral filtering and mellin transform techniques applied to the effect of outer scale on tip/tilt anisoplanatism. *J. Opt. Soc. Am.*, A10:646, 1993.
- [27] M. Tallon and R. Foy. Adaptive telescope with laser probe: isoplanatism and cone effect. *Astronomy and Astrophysics*, 235:549, 1990.
- [28] A. Tokovinin, M. Le Louarn, and M. Sarazin. Isoplanatic angle in a multi-conjugate adaptive optics system. 2000.
- [29] R.K. Tyson. *Principles of Adaptive Optics*. Academic Press, 2nd Edition, 1998.
- [30] G.C. Valley and S.M. Wandzura. Spatial correlation of phase-expansion coefficients for propagation through atmospheric turbulence. *J. Opt. Soc. Am.*, 69,5:712, 1979.

- [31] E.P. Wallner. Optimizing the locations of multiconjugate wavefront correctors. *Proc. SPIE*, 2201:110, 1994.